First-Principles Model-based Robust Control of the Current Profile Evolution in the DIII-D Tokamak

Justin E. Barton, Mark D. Boyer, Wenyu Shi, Eugenio Schuster, Tim C. Luce, John R. Ferron, Michael L. Walker, David A. Humphreys, Ben G. Penaflor and Robert D. Johnson

***Abstract*— Setting up a suitable toroidal current profile in a fusion tokamak reactor is vital to the eventual realization of a commercial nuclear fusion power plant. Creating the desired current profile during the ramp-up and early flat-top phases of the plasma discharge and then actively maintaining this target profile for the remainder of the discharge is the goal at the DIII-D tokamak. The evolution of the toroidal current profile in tokamaks is related to the evolution of the poloidal magnetic flux profile, which is modeled by the magnetic diffusion equation. A simplified first-principles-driven, nonlinear, dynamic, control-oriented, partial differential equation model of the poloidal flux profile evolution is obtained by combining the magnetic diffusion equation with empirical correlations obtained from experimental data at DIII-D and is used to synthesize a robust H_∞ feedback controller to track a desired reference trajectory of the poloidal magnetic flux gradient profile. We employ a singular value decomposition of the static gain matrix of the plant model to identify the most relevant channels which we control with the feedback controller. A framework for real-time feedforward + feedback control was implemented in the DIII-D Plasma Control System and experimental results in the DIII-D tokamak are presented to illustrate the capabilities of the feedback controller. These experiments mark the first time ever a first-principles-driven model-based magnetic profile controller was successfully implemented and tested in a tokamak device.**

I. Introduction

The magnetic confinement approach to nuclear fusion energy production has been extensively researched for many years, and one of the most promising magnetic confinement devices is the tokamak. However, in order for a commercial tokamak power plant to be realized, there are many challenges that need to be overcome, one of which is the ability to operate the tokamak in a "steady state" manner, which requires non-inductive sustainment of the plasma current. Setting up a desirable current profile in the device is essential to one advanced tokamak operating scenario characterized by non-inductive sustainment of the plasma current. The safety factor, or q, profile can be used to specify the current profile in the machine, and active feedback control of the evolution of the q profile at discrete points in the tokamak has been demonstrated at DIII-D [1] during the ramp-up and early flat-top phases of the discharge. Present limitations of the employed non-model-based controller, such as oscillations and instability under certain operating conditions, motivate the design of a model-based controller that takes into account the dynamics of the entire q profile in response to the actuators and has the potential for improved performance.

The poloidal magnetic flux profile evolution, modeled in normalized cylindrical coordinates by a partial differential equation (PDE) called the magnetic diffusion equation, is related to the current profile evolution. A first-principles-driven, control-oriented, PDE model of the poloidal flux profile evolution for low-confinement (L-mode) plasma discharges was developed in [2]. The control strategy we employ to control the q profile evolution is a feedforward + feedback control scheme, where the feedforward and feedback control inputs are computed off-line and on-line respectively. Optimal feedforward control algorithms to achieve the best possible q profile/target matching during the initial phase of the discharge were designed using nonlinear programming [3] and extremum seeking [4]. To add robustness to the control strategy, we add a feedback component to the control scheme, with the goal being to track a desired reference trajectory of the q profile evolution, to reject the effects of external disturbances to the system, and to overcome uncertainties in the model used for control design.

In this work, we extend our previous work [5] in many important areas. Firstly, we consider the problem of designing a feedback controller to track a desired reference trajectory of the poloidal flux gradient profile, which is inversely related to the q profile, instead of regulating the poloidal flux profile around a desired reference trajectory. Secondly, we employ a singular value decomposition of the static gain matrix of the plant model to determine which linear combinations of the plant outputs we can effectively control [6]. Finally, we implemented a framework for real-time control in the DIII-D Plasma Control System (PCS) and tested the feedback controller experimentally in the DIII-D tokamak. These experiments mark the first time ever a first-principles-driven model-based magnetic profile controller was successfully implemented and tested in a tokamak device.

We introduce a PDE model for the poloidal flux gradient profile evolution in section II. In section III, the governing PDE is approximated by a finite dimensional system of ordinary differential equations. The reduced-order model is linearized around the feedforward trajectories of the system, and a linear, time varying state-space system of the deviation dynamics is derived. The time varying system is represented as an uncertain state-space model and formulated into a robust control framework in section IV. In section V, we

This work was supported in part by the National Science Foundation CAREER Award program (ECCS-0645086) and the U.S. Department of Energy (DE-FG02-09ER55064, DE-FC02-04ER54698). J.E. Barton (justin.barton@lehigh.edu), M.D. Boyer, W. Shi, and E. Schuster are with the Department of Mechanical Engineering and Mechanics, Lehigh University, Bethlehem, PA 18015, USA. T.C. Luce, J.R. Ferron, M.L. Walker, D.A. Humphreys, B.G. Penaflor, and R.D. Johnson are with General Atomics, San Diego, CA 92121, USA.

use the nominal model to identify the most relevant control channels, and a robust H_∞ feedback controller is designed to control those channels in section VI. Finally, the feedback controller is tested experimentally in section VII.

II. Current Profile Evolution Model

Any quantity that is constant on each magnetic surface within the tokamak plasma can be used to index the magnetic surfaces. We choose the mean geometric minor radius, ρ, of the magnetic surface, i.e., $\pi B_{\phi,0}\rho^2 = \Phi$, as the indexing variable, where Φ is the toroidal magnetic flux and $B_{\phi,0}$ is the reference magnetic field at the geometric major radius R_0 of the tokamak. The normalized minor radius is defined as $\hat{\rho} = \rho/\rho_b$, where ρ_b is the minor radius of the last closed magnetic surface. Simplified scenario-oriented models for the electron temperature, the plasma resistivity, and the non-inductive current density were identified based on empirical correlations obtained from experimental observations at DIII-D for L-mode discharges [2]. The plasma current is mainly driven by induction in L-mode discharges, therefore, we neglect the effects on the non-inductive bootstrap current. By using these simplified models, the evolution of the poloidal magnetic flux is given by the magnetic diffusion equation

$$\frac{\partial \psi}{\partial t} = f_1(\hat{\rho})u_1(t)\frac{1}{\hat{\rho}}\frac{\partial}{\partial \hat{\rho}}\left(\hat{\rho} f_4(\hat{\rho})\frac{\partial \psi}{\partial \hat{\rho}}\right) + f_2(\hat{\rho})u_2(t) \quad (1)$$

with boundary conditions

$$\left.\frac{\partial \psi}{\partial \hat{\rho}}\right|_{\hat{\rho}=0} = 0 \qquad \left.\frac{\partial \psi}{\partial \hat{\rho}}\right|_{\hat{\rho}=1} = -k_3 u_3(t) \quad (2)$$

where ψ is the poloidal stream function which is closely related to the poloidal magnetic flux Ψ, i.e., $\Psi = 2\pi\psi$, t is the time, $f_1(\hat{\rho})$, $f_2(\hat{\rho})$, and $f_4(\hat{\rho})$ are functions of the simplified models, k_3 is a constant, and

$$u_1(t) = \left(\frac{\bar{n}(t)}{I(t)\sqrt{P_{tot}(t)}}\right)^{3/2},\ u_2(t) = \frac{\sqrt{P_{tot}(t)}}{I(t)},\ u_3(t) = I(t) \quad (3)$$

are the diffusivity, interior, and boundary control actuators respectively, where $I(t)$ is the total plasma current, $P_{tot}(t)$ is the total average neutral beam power injected into the plasma, and $\bar{n}(t)$ is the line average plasma density [2].

The q profile is related to the current profile in the machine and is defined as $q(\rho,t) = -d\Phi/d\Psi$. By using the constant relationship between ρ and Φ, $\pi B_{\phi,0}\rho^2 = \Phi$, and the definition of $\hat{\rho}$, the safety factor is written as $q(\hat{\rho},t) = -[B_{\phi,0}\rho_b^2\hat{\rho}]/[\partial\psi/\partial\hat{\rho}]$. As the q profile is inversely dependent on the poloidal stream function gradient $\partial\psi/\partial\hat{\rho}$, it is chosen to be the controlled variable and is denoted by

$$\theta(\hat{\rho},t) = \partial\psi/\partial\hat{\rho}(\hat{\rho},t). \quad (4)$$

By expanding (1) using the chain rule, inserting (4) into this expanded equation, and differentiating the resulting equation with respect to $\hat{\rho}$, the PDE governing the evolution of $\theta(\hat{\rho},t)$ is found to be

$$\frac{\partial \theta}{\partial t} = \left[h_0(\hat{\rho})\frac{\partial^2\theta}{\partial\hat{\rho}^2} + h_1(\hat{\rho})\frac{\partial\theta}{\partial\hat{\rho}} + h_2(\hat{\rho})\theta\right]u_1(t) + h_3(\hat{\rho})u_2(t) \quad (5)$$

with boundary conditions

$$\theta(0,t) = 0 \qquad \theta(1,t) = -k_3 u_3(t) \quad (6)$$

where $(\cdot)' = d/d\hat{\rho}$, $h_0(\hat{\rho}) = f_1(\hat{\rho})f_4(\hat{\rho})$, $h_1(\hat{\rho}) = f_1'(\hat{\rho})f_4(\hat{\rho}) + f_1(\hat{\rho})f_4(\hat{\rho})/\hat{\rho} + 2f_1(\hat{\rho})f_4'(\hat{\rho})$, $h_2(\hat{\rho}) = f_1'(\hat{\rho})f_4'(\hat{\rho}) + f_1'(\hat{\rho})f_4(\hat{\rho})/\hat{\rho} + f_1(\hat{\rho})f_4'(\hat{\rho})/\hat{\rho} - f_1(\hat{\rho})f_4(\hat{\rho})/\hat{\rho}^2 + f_1(\hat{\rho})f_4''(\hat{\rho})$, and $h_3(\hat{\rho}) = f_2'(\hat{\rho})$. The model (5)-(6) is the starting point for the development of the feedback controller design.

III. Model Reduction

The governing PDE (5) is discretized in space using a truncated Taylor series expansion to approximate the spatial derivatives while leaving the time domain continuous [7] in order to construct a reduced-order model suitable for control design. The non-dimensional domain of interest, [0,1], is represented as l nodes, and the spacing between the nodes, $\Delta\hat{\rho}$, is defined as $\Delta\hat{\rho} = 1/(l-1)$. Central finite difference spatial derivative approximations of $O(\Delta\hat{\rho}^2)$ are used in the interior node region, $2 \le i \le (l-1)$. After applying the spatial derivative approximations to (5) and taking into account the boundary conditions (6), we obtain a matrix representation for the reduced-order model

$$\dot{\alpha}(t) = \Gamma\alpha(t)v_1(t) + \Omega v_2(t) + \Pi v_3(t) \quad (7)$$

where the vector $\alpha = [\theta_2, \ldots, \theta_{l-1}]^T \in \mathbb{R}^{(l-2)\times 1}$ is the state of the system at the interior discrete nodes, the vector

$$[v_1(t), v_2(t), v_3(t)]^T = [u_1(t), u_2(t), u_1(t)u_3(t)]^T \in \mathbb{R}^{3\times 1} \quad (8)$$

is the control input, and $\Gamma \in \mathbb{R}^{(l-2)\times(l-2)}$, $\Omega \in \mathbb{R}^{(l-2)\times 1}$, and $\Pi \in \mathbb{R}^{(l-2)\times 1}$ are the system matrices. The values of θ at the boundary nodes $i = 1$ and $i = l$ are known from (6) and are therefore not included in the reduced-order model (7).

Let $\alpha_{FF}(t)$ and $v_{FF}(t)$ be the feedforward trajectories of the states and control inputs respectively with initial condition $\alpha_{FF}(0)$. These feedforward trajectories satisfy

$$\dot{\alpha}_{FF}(t) = \Gamma\alpha_{FF}(t)v_{1_{FF}}(t) + \Omega v_{2_{FF}}(t) + \Pi v_{3_{FF}}(t). \quad (9)$$

By defining the perturbation variables $x(t) = \alpha(t) - \alpha_{FF}(t)$ and $v_{FB}(t) = v(t) - v_{FF}(t)$, where $x(t)$ is the deviation away from the feedforward state trajectories and $v_{FB}(t)$ is the output of the to-be-designed feedback controller, we can obtain a model suitable for tracking control design. By inserting the fluctuation variables into (7) and using (9), we obtain a nonlinear dynamic model for x. While we preserve the input nonlinearities by the nonlinear transformations (3) and (8), we approximately linearize the state dynamics by neglecting the nonlinear term, i.e., $[\alpha_{FF} + x] \approx \alpha_{FF}$. Simulations and experiments show the closed-loop system to be robust to this approximation. Therefore, the linear, time variant dynamic model for the deviation dynamics is expressed as

$$\dot{x} = A(t)x + B(t)v_{FB} \qquad y = Cx + Dv_{FB} \quad (10)$$

where $A(t) = \Gamma v_{1_{FF}}(t) \in \mathbb{R}^{n\times n}$, $B(t) = [\Gamma\alpha_{FF}(t), \Omega, \Pi] \in \mathbb{R}^{n\times 3}$, $C = I_n \in \mathbb{R}^{n\times n}$ where I_n is an $n \times n$ identity matrix, $D = 0 \in \mathbb{R}^{n\times 3}$, $x \in \mathbb{R}^{n\times 1}$, $y \in \mathbb{R}^{n\times 1}$, $v_{FB} = [v_{1_{FB}}, v_{2_{FB}}, v_{3_{FB}}]^T \in \mathbb{R}^{3\times 1}$, and $n = l - 2$. Here α, and therefore x, is assumed measurable.

IV. Model in Robust Control Framework

A linear system with state-space matrices A, B, C, and D has a transfer function representation $G(s) = C(sI_n - A)^{-1}B + D$ where s denotes the Laplace variable. By defining the matrix

$$M_a = \begin{bmatrix} A & B \\ C & D \end{bmatrix} \tag{11}$$

the system transfer function can be written as an upper linear fractional transformation (LFT) as $G(s) = F_u(M_a, [1/s]I_n) = D + C(sI_n - A)^{-1}B$, where F_u denotes the upper LFT. The time varying parameters $v_{1_{FF}}(t)$ and $\alpha_{FF}(t)$ in the definition of the system matrices of (10) are chosen to be modeled as a time varying uncertainty as

$$v_{1_{FF}}(t) \in \gamma_v\Big(1 + \beta_v\delta_v\Big) \quad \alpha_{i_{FF}}(t) \in \gamma_\alpha^i\Big(1 + \beta_\alpha^i\delta_\alpha^i\Big) \tag{12}$$

where $\gamma_v = (v_{1_{FF_{max}}} + v_{1_{FF_{min}}})/2$, $\gamma_\alpha^i = (\alpha_{i_{FF_{max}}} + \alpha_{i_{FF_{min}}})/2$, $\beta_v = (v_{1_{FF_{max}}} - v_{1_{FF_{min}}})/(2\gamma_v)$, and $\beta_\alpha^i = (\alpha_{i_{FF_{max}}} - \alpha_{i_{FF_{min}}})/(2\gamma_\alpha^i)$ with $|\delta_v| \leq 1$ and $|\delta_\alpha^i| \leq 1$ where $i = 1, 2, \ldots, n$. By employing (12) and defining the total uncertainty vector as $\delta = [\delta_\alpha^1, \ldots, \delta_\alpha^n, \delta_v] \in \mathbb{R}^{(n+1)\times 1}$, the matrix M_a is written in the form of a general affine state-space uncertainty

$$M_a = \begin{bmatrix} A_0 + \sum_{m=1}^{n+1} \delta_m A_m^* & B_0 + \sum_{m=1}^{n+1} \delta_m B_m^* \\ C_0 + \sum_{m=1}^{n+1} \delta_m C_m^* & D_0 + \sum_{m=1}^{n+1} \delta_m D_m^* \end{bmatrix} \tag{13}$$

where

$$A_0 = \gamma_v\Gamma \quad B_{0_k} = \left[\sum_{i=1}^{n} \gamma_\alpha^i \Gamma_{k,i}, \Omega_k, \Pi_k\right] \quad C_0 = I_n \quad D_0 = 0 \tag{14}$$

and

$$\begin{gathered} A_{1,2,\ldots,n}^* = 0 \qquad A_{n+1}^* = \gamma_v\beta_v\Gamma \\ B_{m_k}^* = \left[(\gamma_\alpha^m\beta_\alpha^m)\Gamma_{k,m}, 0, 0\right] \quad \text{for } m = 1, 2, \ldots, n \quad B_{n+1}^* = 0 \\ C_{1,2,\ldots,n+1}^* = 0 \qquad D_{1,2,\ldots,n+1}^* = 0 \end{gathered} \tag{15}$$

where $k = 1, 2, \ldots, n$, $\Gamma_{k,i}$ denotes the k-th row i-th column component of Γ, B_{0_k} and $B_{m_k}^*$ denote the k-th component of B_0 and B_m^* respectively, and δ_m denotes the m-th component of δ.

By exploiting the structure of the state matrices in (13) and using singular value decomposition, the feedback system can be expressed in the conventional $P - \Delta$ control framework by employing the method outlined in [8]. See [5] for an example of this technique. If the plant $P \in \mathbb{R}^{(q_T+n)\times(q_T+3)}$, where q_T is the rank of the structured uncertainty matrix $\Delta = \text{diag}\{\delta\}$, is partitioned as

$$P = \begin{bmatrix} P_{11} & P_{12} \\ P_{21} & P_{22} \end{bmatrix} \tag{16}$$

the input-output equations of the system are

$$y_\Delta = P_{11}u_\Delta + P_{12}v_{FB} \qquad y = P_{21}u_\Delta + P_{22}v_{FB} \tag{17}$$

where $P_{11} \in \mathbb{R}^{q_T\times q_T}$, $P_{12} \in \mathbb{R}^{q_T\times 3}$, $P_{21} \in \mathbb{R}^{n\times q_T}$, $P_{22} \in \mathbb{R}^{n\times 3}$, $y_\Delta \in \mathbb{R}^{q_T\times 1}$, $u_\Delta \in \mathbb{R}^{q_T\times 1}$, $y \in \mathbb{R}^{n\times 1}$, and $v_{FB} \in \mathbb{R}^{3\times 1}$.

V. Identification of Relevant Control Channels

It is desired that the output $y(t)$ be able to track a reference value $r(t)$, therefore, we define the tracking error $e(t)$ as

$$e(t) = r(t) - y(t). \tag{18}$$

The conditions to bring the tracking error exactly to zero are typically not met because the number of controlled outputs n is larger than the number of controlled inputs 3. As a result, we can only independently control 3 linear combinations of the output of the system, and we employ a technique based on the singular value decomposition of the static gain matrix of the nominal state-space system A_0, B_0, C_0, D_0 to identify the most relevant control channels. The relationship between the outputs y and the inputs v_{FB} of the nominal system is expressed as $y = G_0(s)v_{FB}$ where $G_0(s) = C_0(sI_n - A_0)^{-1}B_0 + D_0$ is the nominal transfer function.

To begin the process of determining the relevant channels, we consider a steady state performance index defined as

$$\bar{J} = \lim_{t\to\infty} e^T(t)Qe(t) = \bar{e}^T Q\bar{e} \tag{19}$$

where $\bar{e}$ denotes the steady state tracking error, $(\cdot)^T$ denotes the matrix transpose, and $Q \in \mathbb{R}^{n\times n}$ is a symmetric positive definite weighting matrix. Assuming a constant reference $\bar{r}$ and provided the closed-loop system is internally stable, the system can be maintained at steady state. Under these assumptions, the input-output relation in steady state is expressed as

$$\bar{y} = \bar{G}_0\bar{v}_{FB} = \big(-C_0(A_0)^{-1}B_0 + D_0\big)\bar{v}_{FB} \tag{20}$$

where $\bar{y}$ denotes the steady state output, $\bar{v}_{FB}$ denotes the steady state input, and $\bar{G}_0$ denotes the steady state gain of the plant $G_0(s)$ (i.e., $s \to 0$). We introduce another positive definite weighting matrix $R \in \mathbb{R}^{3\times 3}$ in order to also weight the control effort, and we define the "weighted" steady state transfer function $\tilde{G}_0$ and its "economy" size singular value decomposition [9] as

$$\tilde{G}_0 = Q^{1/2}\bar{G}_0R^{-1/2} = U\Sigma V^T \tag{21}$$

where $\Sigma = \text{diag}(\sigma_1, \sigma_2, \sigma_3) \in \mathbb{R}^{3\times 3}$ is a diagonal matrix of steady state singular values and $U \in \mathbb{R}^{n\times 3}$ and $V \in \mathbb{R}^{3\times 3}$ are unitary matrices. By employing (21), the steady state input-output relation (20) is expressed as

$$\bar{y} = Q^{-1/2}\tilde{G}_0R^{1/2}\bar{v}_{FB} = Q^{-1/2}U\Sigma V^TR^{1/2}\bar{v}_{FB}. \tag{22}$$

We note that the columns of the matrix $Q^{-1/2}U\Sigma$ define a basis for the subspace of obtainable steady state output values, and as a result, we can write

$$\bar{y} = Q^{-1/2}U\Sigma\bar{y}^* \Longleftrightarrow \bar{y}^* = \Sigma^{-1}U^TQ^{1/2}\bar{y} \tag{23}$$

where $\bar{y}^* \in \mathbb{R}^{3\times 1}$. This implies that only the component of the reference vector $\bar{r}$ that lies in this subspace will be able to be tracked in steady state. Therefore, the reference vector is decomposed as $\bar{r} = \bar{r}_t + \bar{r}_{nt}$ where $\bar{r}_t$ is the trackable component and $\bar{r}_{nt}$ is the non-trackable component. The reference vector components are then defined as

$$\bar{r}_t = Q^{-1/2}U\Sigma\bar{r}^* \Longleftrightarrow \bar{r}^* = \Sigma^{-1}U^TQ^{1/2}(\bar{r}_t + \bar{r}_{nt}) \tag{24}$$

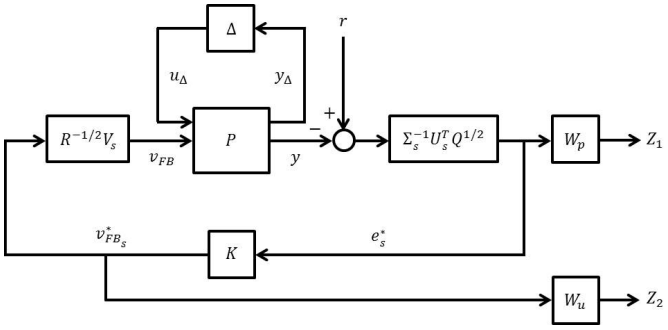

Fig. 1. Schematic of control problem formulation.

with $\bar{r}^* \in \mathbb{R}^{3\times 1}$ and $\Sigma^{-1}U^TQ^{1/2}\bar{r}_{nt} = 0$. By defining $\bar{v}^*_{FB} = V^TR^{1/2}\bar{v}_{FB} \in \mathbb{R}^{3\times 1}$, a one-to-one relationship between the outputs $\bar{y}^*$ and the inputs $\bar{v}^*_{FB}$ is obtained by using (23) and (22) as

$$\bar{y}^* = \Sigma^{-1}U^TQ^{1/2}\bar{y} = \Sigma^{-1}U^TQ^{1/2}Q^{-1/2}U\Sigma V^TR^{1/2}\bar{v}_{FB} = \bar{v}^*_{FB}. \tag{25}$$

The steady state error is now written as $\bar{e} = \bar{r} - \bar{y} = Q^{-1/2}U\Sigma(\bar{r}^* - \bar{y}^*)$ and the performance index (19) is expressed as

$$\bar{J} = \bar{e}^TQ\bar{e} = \left(\bar{r}^* - \bar{y}^*\right)^T\Sigma^2\left(\bar{r}^* - \bar{y}^*\right) = \sum_{i=1}^{3}\sigma_i^2\left(\bar{r}^*_i - \bar{y}^*_i\right)^2 \tag{26}$$

where σ_i denotes the i-th singular value, $\bar{r}^*_i$ denotes the i-th component of $\bar{r}^*$, and $\bar{y}^*_i$ denotes the i-th component of $\bar{y}^*$.

We note that the i-th singular value acts as a weight parameter for the i-th component of the tracking error in (26). It is possible that two sequential singular values could exhibit a large difference in magnitude, i.e., $\sigma_i \gg \sigma_{i+1}$. As a result, if we take all of the singular values into account, we could spend a lot of control effort for only a small improvement in the value of the performance index (26). To avoid this penalty, we partition the singular values into k significant singular values Σ_s and $3-k$ negligible singular values Σ_{ns} and introduce the partitions

$$U = \begin{bmatrix}U_s & U_{ns}\end{bmatrix} \qquad V = \begin{bmatrix}V_s & V_{ns}\end{bmatrix} \qquad \Sigma = \begin{bmatrix}\Sigma_s & 0\\ 0 & \Sigma_{ns}\end{bmatrix} \tag{27}$$

$$\bar{r}^* = \begin{bmatrix}\bar{r}^*_s\\ \bar{r}^*_{ns}\end{bmatrix} \qquad \bar{y}^* = \begin{bmatrix}\bar{y}^*_s\\ \bar{y}^*_{ns}\end{bmatrix} \qquad \bar{v}^*_{FB} = \begin{bmatrix}\bar{v}^*_{FB_s}\\ \bar{v}^*_{FB_{ns}}\end{bmatrix} \tag{28}$$

where $U_s \in \mathbb{R}^{n\times k}$, $\Sigma_s \in \mathbb{R}^{k\times k}$, $V_s \in \mathbb{R}^{3\times k}$, $\bar{r}^*_s \in \mathbb{R}^{k\times 1}$, $\bar{y}^*_s \in \mathbb{R}^{k\times 1}$, and $\bar{v}^*_{FB_s} \in \mathbb{R}^{k\times 1}$. Using (27) and (28), a reduced form of the performance index (26) is written as

$$\bar{J}_s = \left(\bar{r}^*_s - \bar{y}^*_s\right)^T\Sigma_s^2\left(\bar{r}^*_s - \bar{y}^*_s\right) = \sum_{i=1}^{k}\sigma_i^2\left(\bar{r}^*_i - \bar{y}^*_i\right)^2 \tag{29}$$

where

$$\bar{r}^*_s = \Sigma_s^{-1}U_s^TQ^{1/2}(\bar{r}_t + \bar{r}_{nt}) \qquad \bar{y}^*_s = \Sigma_s^{-1}U_s^TQ^{1/2}\bar{y}. \tag{30}$$

By employing (30) and (22), a reduced form of the decoupled system (25) is expressed as

$$\bar{y}^*_s = \Sigma_s^{-1}U_s^TQ^{1/2}\bar{y} = \Sigma_s^{-1}U_s^TQ^{1/2}Q^{-1/2}U\Sigma V^TR^{1/2}\bar{v}_{FB} = \bar{v}^*_{FB_s} \tag{31}$$

where we have defined $\bar{v}^*_{FB_s} = V_s^TR^{1/2}\bar{v}_{FB}$.

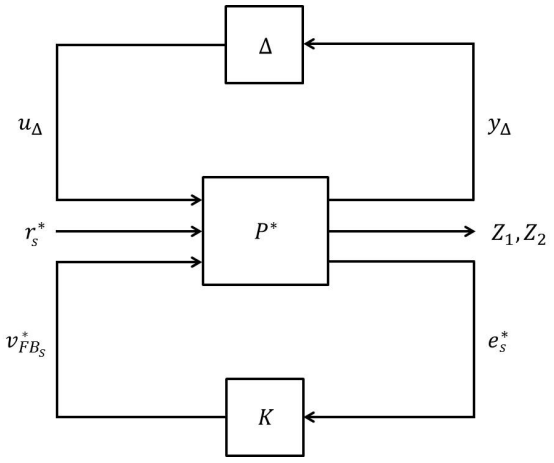

Fig. 2. Model in $\Delta - P^* - K$ robust control design framework.

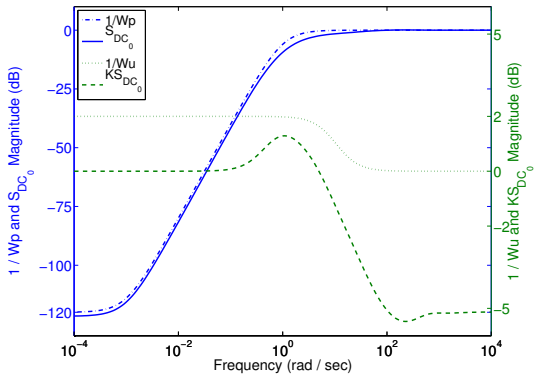

Fig. 3. Maximum singular value diagram of: inverse of performance weight $1/W_p$ (dash-dot), transfer function S_{DC_o} (solid), inverse of performance weight $1/W_u$ (dot), and transfer function KS_{DC_o} (dash).

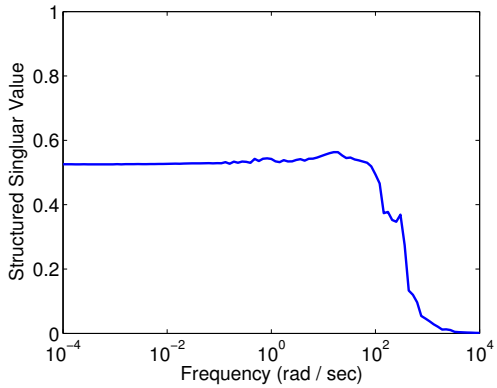

Fig. 4. Structured singular value μ versus frequency.

VI. Controller Synthesis

The control goal is to design a feedback controller that can minimize the tracking error (18) while using as little feedback control effort as possible, achieve a set of specified performance objectives, and robustly stabilize the system by controlling the significant portion of the output of the system (17). A schematic of this control problem is shown in Figure 1 where K is the feedback controller, $Z_1 = W_pe^*_s$, $Z_2 = W_uv^*_{FB_s}$, and W_p and W_u are frequency dependent weight functions. The feedback system is expressed in the conventional $\Delta - P^* - K$ robust control design framework shown in Figure 2 where P^* is the generalized plant. By defin-

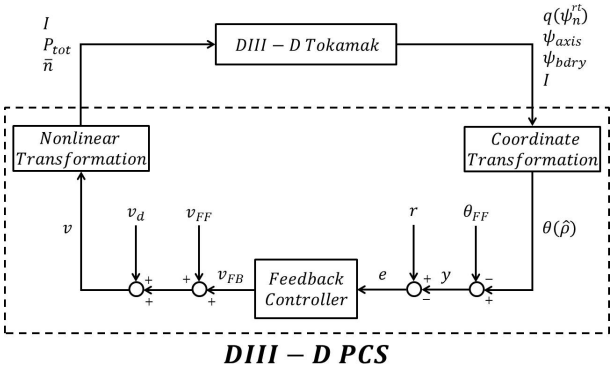

Fig. 5. DIII-D tokamak configuration with DIII-D PCS real-time code.

ing the transfer functions $G_{DC} = \Sigma_s^{-1} U_s^T Q^{1/2} P_{22} R^{-1/2} V_s$, $T_{y_\Delta v} = P_{12} R^{-1/2} V_s$, and $T_{y u_\Delta} = \Sigma_s^{-1} U_s^T Q^{1/2} P_{21}$, the input-output equations of the generalized plant P^* are

$$\left[\begin{array}{c} y_\Delta \\ Z_1 \\ Z_2 \\ \hline e_s^* \end{array}\right] = \left[\begin{array}{cc|c} P_{11}^* & P_{12}^* & P_{13}^* \\ P_{21}^* & P_{22}^* & P_{23}^* \\ P_{31}^* & P_{32}^* & P_{33}^* \\ \hline P_{41}^* & P_{42}^* & P_{43}^* \end{array}\right] \left[\begin{array}{c} u_\Delta \\ r_s^* \\ \hline v_{FB_s}^* \end{array}\right] = \left[\begin{array}{c|c} \tilde{P}_{11}^* & \tilde{P}_{12}^* \\ \hline \tilde{P}_{21}^* & \tilde{P}_{22}^* \end{array}\right] \left[\begin{array}{c} u_\Delta \\ r_s^* \\ \hline v_{FB_s}^* \end{array}\right] \tag{32}$$

where

$$\begin{array}{lll} P_{11}^* = P_{11} & P_{21}^* = -W_p T_{y u_\Delta} & P_{31}^* = 0 \\ P_{12}^* = 0 & P_{22}^* = W_p & P_{32}^* = 0 \\ P_{13}^* = T_{y_\Delta u} & P_{23}^* = -W_p G_{DC} & P_{33}^* = W_u \\ P_{41}^* = -T_{y u_\Delta} & P_{42}^* = I & P_{43}^* = -G_{DC}. \end{array}$$

The system (32) can be written in the $N-\Delta$ control analysis configuration by using the definition of the lower LFT, which is denoted as F_l, between P^* and K, i.e., $N = F_l(P^*, K) = \tilde{P}_{11}^* + \tilde{P}_{12}^* K (I - \tilde{P}_{22}^* K)^{-1} \tilde{P}_{21}^*$. By using the definitions $S_{DC_O} = (I + G_{DC} K)^{-1}$, $T_{DC_O} = G_{DC} K (I + G_{DC} K)^{-1}$, and $I = S_{DC_O} + T_{DC_O}$, the feedback system is written as

$$\begin{bmatrix} y_\Delta \\ Z_1 \\ Z_2 \end{bmatrix} = N \begin{bmatrix} u_\Delta \\ \bar{r}_s^* \end{bmatrix} \quad N = \begin{bmatrix} P_{11} - T_{y_\Delta v} K S_{DC_O} T_{y u_\Delta} & T_{y_\Delta v} K S_{DC_O} \\ -W_p S_{DC_O} T_{y u_\Delta} & W_p S_{DC_O} \\ -W_u K S_{DC_O} T_{y u_\Delta} & W_u K S_{DC_O} \end{bmatrix}.$$

The nominal performance condition of the closed-loop system and the control problem are expressed as

$$\begin{bmatrix} Z_1 \\ Z_2 \end{bmatrix} = \begin{bmatrix} W_p S_{DC_O} \\ W_u K S_{DC_O} \end{bmatrix} \left[\bar{r}_s^*\right] \quad \Rightarrow \quad \min_K \left\| \begin{matrix} W_p S_{DC_O} \\ W_u K S_{DC_O} \end{matrix} \right\|_\infty, \quad \forall \omega \tag{33}$$

where $||\cdot||_\infty$ denotes the H_∞ norm. The frequency dependent weight functions $W_p(s)$ and $W_u(s)$ are chosen to shape the closed-loop transfer functions and are parameterized as [10]

$$W_p(s) = \frac{\left(s/\sqrt{M_p} + \omega_p\right)^2}{\left(s + \omega_p \sqrt{H_p^*}\right)^2} \qquad W_u(s) = \frac{\left(s/\sqrt{M_u} + \omega_u\right)^2}{\left(s + \omega_u \sqrt{H_u^*}\right)^2} \tag{34}$$

where $M_p = 1$, $H_p^* = 10^{-6}$, $\omega_p = 1$, $M_u = 1$, $H_u^* = 10^{0.1}$, and $\omega_u = 10$. The feedback controller K found by solving (33) is written in state-space form as

$$\dot{x}_c = A_c x_c + B_c e_s^* \qquad v_{FB_s}^* = C_c x_c + D_c e_s^* \tag{35}$$

where the vector $x_c \in \mathbb{R}^{p \times 1}$ is the internal controller states, $A_c \in \mathbb{R}^{p \times p}$, $B_c \in \mathbb{R}^{p \times 1}$, $C_c \in \mathbb{R}^{1 \times p}$, and $D_c \in \mathbb{R}^{1 \times 1}$ are the controller system matrices, and p is the number of controller states. For this controller design, the significant singular values were chosen as $\Sigma_s = \sigma_1$. To analyze the closed-loop performance of the nominal system, the maximum singular value diagrams of the inverse of the weight functions and the achieved transfers are computed and are shown in Figure 3. As can be seen from the figure, the desired shapes of the transfer functions S_{DC_O} and KS_{DC_O} are achieved.

To analyze the robust stability of the closed-loop system, the structure of the uncertainty in the $N-\Delta$ control analysis framework is now taken into account. Because the uncertainty has a defined structure, $\Delta = \text{diag}\{\delta\}$, we can define the structured singular value μ as

$$\mu\big(N_{11}(j\omega)\big) = \frac{1}{\min\{k_m | \det(I - k_m N_{11} \Delta) = 0\}} \tag{36}$$

where N_{11} is the transfer function between y_Δ and u_Δ. The closed-loop system is robustly stable for all allowable perturbations if and only if $\mu\big(N_{11}(j\omega)\big) < 1$, $\forall \omega$ [10]. Figure 4 shows a plot of μ versus frequency, and as can be seen from the figure $\mu < 1$, $\forall \omega$. Finally, the multi-input-multi-output feedback controller $\hat{K} \in \mathbb{R}^{3 \times n}$ is expressed as

$$\begin{aligned} \dot{x}_c &= A_c x_c + B_c \Sigma_s^{-1} U_s^T Q^{1/2} e \\ v_{FB} &= R^{-1/2} V_s C_c x_c + R^{-1/2} V_s D_c \Sigma_s^{-1} U_s^T Q^{1/2} e. \end{aligned} \tag{37}$$

A general framework for real-time feedforward + feedback control of magnetic and kinetic plasma profiles has been implemented in the DIII-D PCS as shown in Figure 5. The feedback portion of the controller was implemented as a discrete time state-space controller with a sampling time of 20 milliseconds and was interfaced with the real-time equilibrium reconstruction code in the DIII-D PCS [11] via the Coordinate Transformation block. The Nonlinear Transformation block converts the feedforward + feedback control input to the physical control actuator signals. It is important to note that the requests made by the control algorithm are the references to the control loops commanding the physical actuators. This PCS configuration provides us the ability to test the feedback controller in reference tracking and disturbance rejection experiments. A simulation simserver of the magnetic diffusion equation that can interface with the DIII-D PCS was developed to test the real-time code implemented in the DIII-D PCS [12] where the simulation simserver replaces the DIII-D tokamak in Figure 5.

VII. Experimental Reference Tracking Results

The actuators used to manipulate the poloidal flux gradient profile evolution $\theta(\hat{\rho}, t)$ have a limited ability to drive the system towards a desired target profile based on the physical design of the DIII-D tokamak. As a result, there are a limited number of target profiles that are physically achievable by the machine no matter what type of profile control strategy is employed. The control actuators themselves are also physically constrained in magnitude as well as rate of change, which further reduces the range of target profiles achievable for a given initial θ profile. The goal of the experimental test was to verify that the feedback controller synthesized from

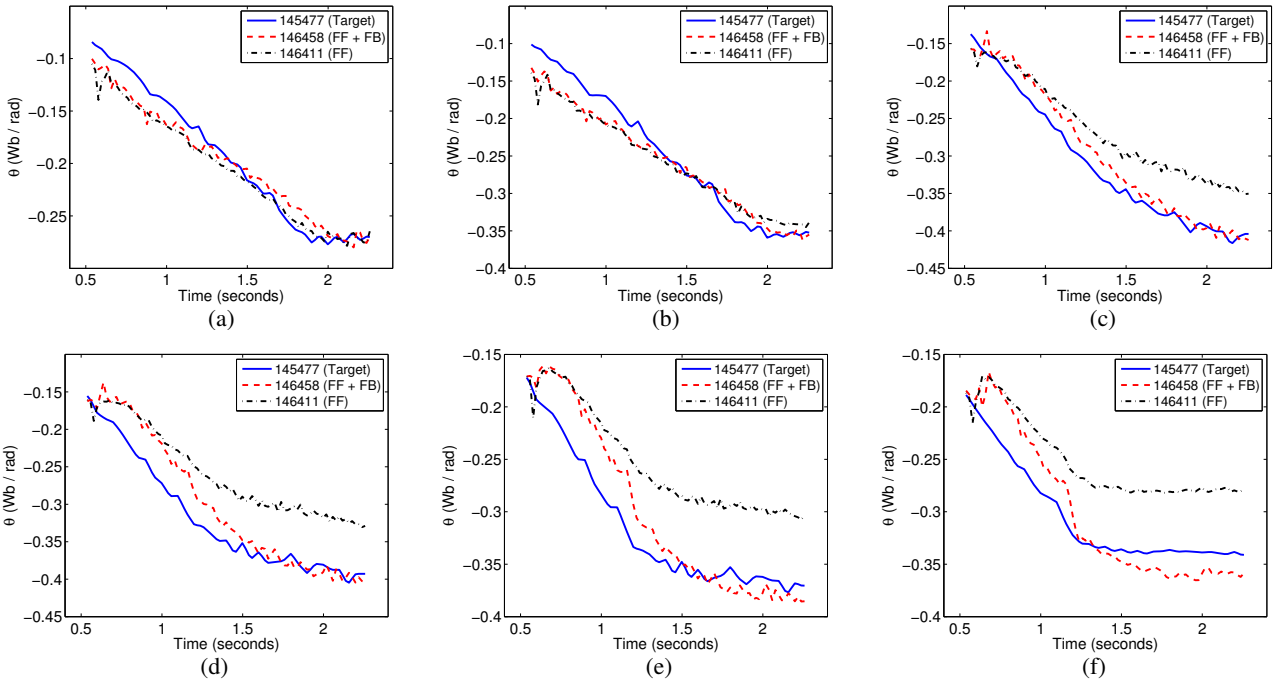

Fig. 6. Time trace of poloidal flux gradient θ at normalized radii (a) $\hat{\rho} = 0.3$, (b) $\hat{\rho} = 0.4$, (c) $\hat{\rho} = 0.6$, (d) $\hat{\rho} = 0.7$, (e) $\hat{\rho} = 0.8$, and (f) $\hat{\rho} = 0.9$.

a first principles based model of the poloidal flux profile evolution is able to drive the system to a target profile that is physically achievable by the machine.

In this section, we experimentally test the reference tracking capabilities of the feedback controller in the DIII-D tokamak. First, we obtained a target poloidal flux gradient profile evolution $\theta_{tar}(\hat{\rho},t)$ that was physically achievable by the machine by executing a feedfoward control only discharge with a nominal set of feedforward control inputs in DIII-D shot # 145477. Another feedforward control discharge was executed with a second set of feedfoward control inputs to generate a second profile evolution $\theta_{FF}(\hat{\rho},t)$ in DIII-D shot # 146411. Finally, in DIII-D shot # 146458, the feedforward actuator trajectories from DIII-D shot # 146411 were combined with the feedback controller (37) in a feedforward + feedback control discharge to track the target profile evolution $\theta_{tar}(\hat{\rho},t)$. The feedback controller was on for the duration of the discharge, and the reference vector was set according to $r(\hat{\rho},t) = \theta_{tar}(\hat{\rho},t) - \theta_{FF}(\hat{\rho},t)$.

For the DIII-D discharges used to test the feedback controller, the ramp-up phase is associated with the time $t = [0.5, 1.2]$ seconds, and the early flat-top phase corresponds to the time $t = [1.2, 2.25]$ seconds. Time traces of θ, at various normalized radii $\hat{\rho}$, achieved during shot #'s 145477 (target), 146458 (feedforward + feedback), and 146411 (feedforward) are shown in Figure 6. The feedback controller can manipulate the θ profile evolution through diffusivity, interior, and boundary actuation. Due to the fact that the boundary actuation is one of the more influential actuators, the feedback controller can more effectively control the θ profile near the plasma boundary because of the spatial proximity of the actuator and the controlled quantity. Therefore, a tracking error in the interior of the plasma will take longer to eliminate

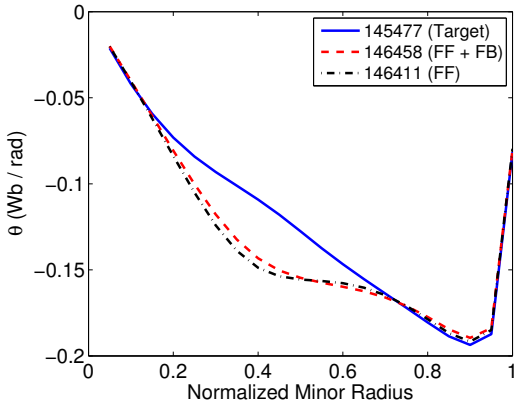

Fig. 7. Initial poloidal flux gradient $\theta(\hat{\rho})$ profile at time $t = 0.538$ seconds.

because the control action applied at the plasma boundary will have to diffuse towards the center of the plasma. This behavior is shown in Figures 6(c)-6(f) for the time traces of θ at normalized radii $\hat{\rho} = 0.6$, 0.7, 0.8, and 0.9 achieved in the feedforward + feedback control discharge. During this discharge, the θ evolution at $\hat{\rho} = 0.6$ and 0.7 is initially below the desired target evolution. Therefore, the feedback controller causes θ at $\hat{\rho} = 0.8$ and 0.9 to overshoot the desired target evolution at these spatial locations in order to cause the θ evolution at $\hat{\rho} = 0.6$ and 0.7 to increase towards the target evolution through diffusion. Once the target θ evolution is achieved at $\hat{\rho} = 0.6$ and 0.7 at the time $t = 2.0$ seconds as shown in Figures 6(c) and 6(d), the feedback controller begins to reduce the tracking error at the normalized radii $\hat{\rho} = 0.8$ and 0.9 during the time interval $t = [2.0, 2.25]$ seconds as shown in Figures 6(e) and 6(f).

Due to the nonlinear behavior of the tokamak plasma and the physical limitations of the actuators to manipulate the θ profile evolution, there is no guarantee that the feedback

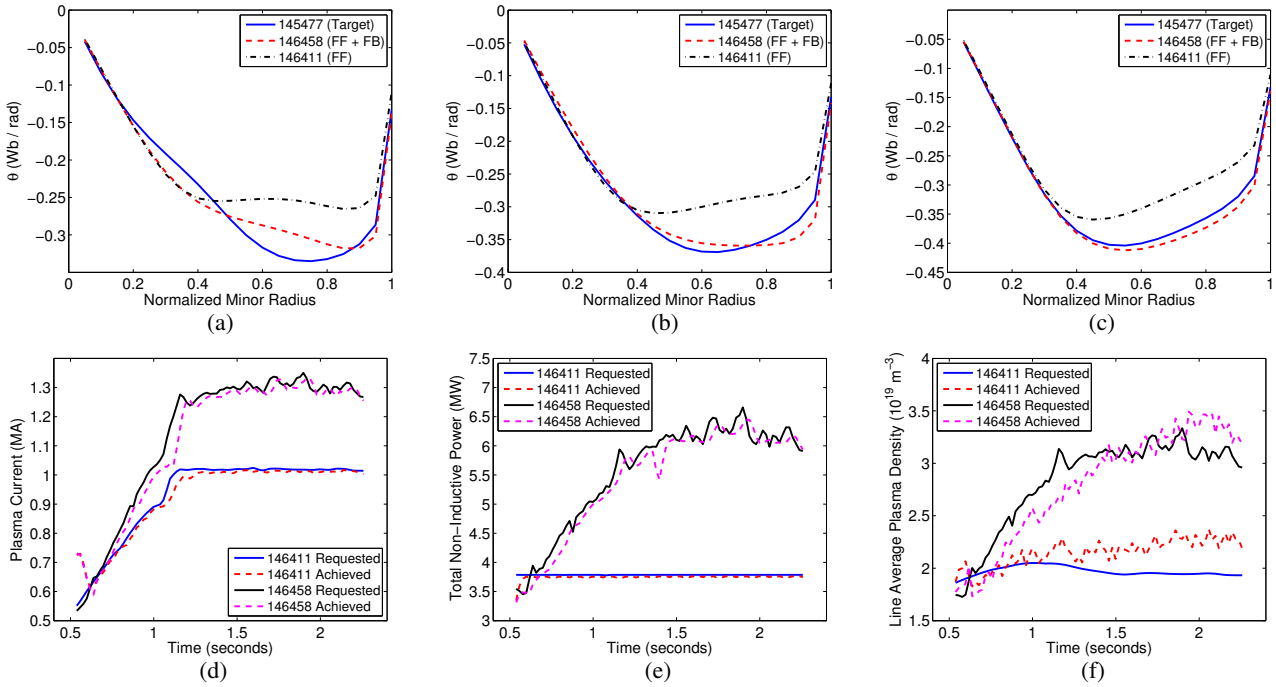

Fig. 8. Poloidal flux gradient $\theta(\hat{\rho})$ profile at time (a) $t = 1.218$ seconds, (b) $t = 1.618$ seconds, and (c) $t = 2.258$ seconds and control trajectory comparison: (d) plasma current (MA), (e) total non-inductive power (MW), and (f) line average density (10^{19} m^{-3}).

controller will be able to drive the θ profile evolution in the feedforward + feedback control discharge to the target profile evolution from the perturbed initial condition shown in Figure 7. The poloidal flux gradient profile $\theta(\hat{\rho})$ matching comparison between shots #'s 145477 (target profile), 146458 (feedforward + feedback), and 146411 (feedforward) at times $t = 1.218$, $t = 1.618$ and $t = 2.258$ seconds is shown in Figures 8(a)-8(c). At the beginning of the ramp-up phase, the feedback controller begins to drive the plasma from the θ profile evolution in shot # 146411 towards the target profile evolution by modifying the feedforward actuator trajectories from shot # 146411. At the end of the early flat-top phase, the feedback controller is able to drive the θ profile in shot # 146458 as close as possible to the target profile achieved in shot # 145477 as shown in Figure 8(c).

A comparison of the actuator trajectories requested by the control algorithm and achieved by the physical actuators for $I(t)$, $P_{tot}(t)$, and $\bar{n}(t)$ in shot #'s 146411 and 146458 is shown in Figures 8(d)-8(f). To track the target profile evolution, the feedback component of the combined controller modifies the feedforward actuator trajectories from shot # 146411 throughout shot # 146458. Also shown in Figures 8(d)-8(f) is the ability of the control loops commanding the physical actuators to follow the requests made by the control algorithm. The control loops commanding the total plasma current and the total average neutral beam power are able to follow the requests very well, and the control loop commanding the line average density is able to follow the request reasonably well.

VIII. Conclusions and Future Work

A robust H_∞ feedback controller was synthesized to control the current profile evolution in the DIII-D tokamak by employing a first-principles-driven model of the poloidal flux profile evolution. The feedback controller was successfully implemented in the DIII-D PCS, interfaced with the available real-time measurements, and successfully tested experimentally. Our future work will consist of developing a control-oriented model of the poloidal flux profile evolution valid in high-confinement (H-mode) plasma discharges that incorporates the effects of the self-generated, non-inductive source of current in the plasma that arises from achieving the desired shape of the q profile in the tokamak machine.

References

[1] J. Ferron *et al.*, "Feedback Control of the Safety Factor Profile Evolution during Formation of an Advanced Tokamak Discharge," *Nuclear Fusion*, vol. 46, no. 10, pp. L13–17, 2006.

[2] Y. Ou *et al.*, "Towards Model-Based Current Profile Control at DIII-D," *Fusion Engineering and Design*, vol. 82, pp. 1153–1160, 2007.

[3] C. Xu *et al.*, "Ramp-Up Phase Current Profile Control of Tokamak Plasmas via Nonlinear Programming," *IEEE Transactions on Plasma Science*, vol. 38, pp. 163–173, 2010.

[4] Y. Ou *et al.*, "Design and Simulation of Extremum-Seeking Open-Loop Optimal Control of Current Profile in the DIII-D Tokamak," *Plasma Physics and Controlled Fusion*, vol. 50, p. 115001, 2008.

[5] J. Barton *et al.*, "Poloidal Magnetic Flux Profile Control in Tokamaks via Normalized Coprime Factorization Robust Control," in *IEEE MSC Conference Proceedings*, 2011, pp. 49–54.

[6] G. Ambrosino *et al.*, "Design and Implementation of an Output Regulation Controller for the JET Tokamak," *IEEE Transactions on Control Systems Technology*, vol. 16, no. 6, pp. 1101–1111, 2008.

[7] W. Schiesser, *The Numerical Method of Lines: Integration of Partial Differential Equations*. Academic Press, San Diego, 1991.

[8] A. Packard, "Whats New with μ: Structured Uncertainty in Multivariable Control," Ph.D. dissertation, Univ. of Calif., Berkeley, 1988.

[9] G. Golub and C. F. Van Loan, *Matrix Computations, 3rd Ed.* Baltimore, Maryland: Johns Hopkins University Press, 1996.

[10] S. Skogestad and I. Postlethwaite, *Multivariable Feedback Control Analysis and Design*. John Wiley & Sons Ltd, 2005.

[11] J. Ferron *et al.*, "Real Time Equilibrium Reconstruction for Tokamak Discharge Control," *Nuclear Fusion*, vol. 38, pp. 1055–1066, 1998.

[12] J. Barton *et al.*, "Simserver Simulation of a Model-based Current Profile Controller in the DIII-D Plasma Control System," *Fusion Engineering and Design*, vol. 86, no. 6-8, pp. 1116–1119, 2011.